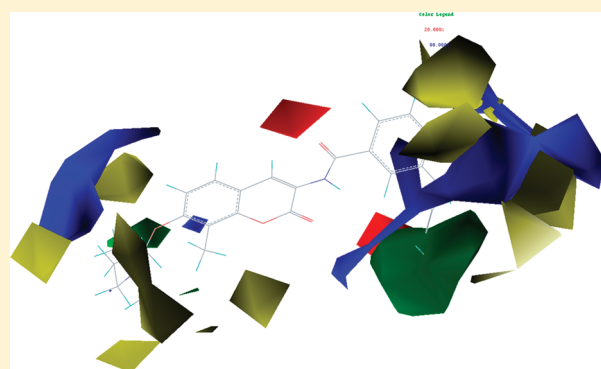


Molecular Design of Anticancer Drug Leads Based on Three-Dimensional Quantitative Structure–Activity Relationship

Xiao Yan Huang, Zhi Jie Shan, Hong Lin Zhai,* Li Na Li, and Xiao Yun Zhang

College of Chemistry and Chemical Engineering, Lanzhou University, Lanzhou, 730000, People's Republic of China

ABSTRACT: Heat shock protein 90 (Hsp90) takes part in the developments of several cancers. Novobiocin, a typically C-terminal inhibitor for Hsp90, will probably used as an important anticancer drug in the future. In this work, we explored the valuable information and designed new novobiocin derivatives based on a three-dimensional quantitative structure–activity relationship (3D QSAR). The comparative molecular field analysis and comparative molecular similarity indices analysis models with high predictive capability were established, and their reliabilities are supported by the statistical parameters. Based on the several important influence factors obtained from these models, six new novobiocin derivatives with higher inhibitory activities were designed and confirmed by the molecular simulation with our models, which provide the potential anticancer drug leads for further research.



1. INTRODUCTION

Over the past few years, molecular chaperones have been focused as the most important topic in biology, since they were found to play an essential role in apoptosis as well as coenzyme. Molecular chaperons are responsible for maintaining the appropriate folding and three-dimensional (3D) conformation of proteins in the cell and also control the balance between the synthesis and the degradation of many proteins.¹ Heat shock protein 90 (Hsp90), which takes part in the development of several cancers, such as breast, colon, pancreatic, and prostatic cancers,² is an ATP-dependent molecular chaperone with exciting new targets.^{3–6} Growing a number of natural products, synthetic and semisynthetic drugs, Hsp90 inhibitors have been developed, which mainly combine the targets of the N-terminal ATP-binding pockets, and present potent antiproliferative affects.^{7–9} However, the potential clinical utility of several N-terminal inhibitors as anticancer drugs was insecure due to their adverse hepatotoxic influences and the encouraging expression of cytoprotective proteins for Hsp90 and Hsp70.^{10–12} Many experimental facts indicate that Hsp90 contains a previously unrecognized C-terminal ATP-binding domain,^{13–15} which has led several research groups to pursue the development of specific C-terminal Hsp90 inhibitors as potential anticancer drug modalities.^{2,12,16–18} Novobiocin, a natural product separated from soil samples containing *Streptomyces spheroids*,¹⁹ is typically a C-terminal Hsp90 inhibitor and stands a good chance of becoming anticancer drug in the future.^{20,21} Nowadays, a series of novobiocin derivatives with high-inhibitory activity were synthesized.^{17,22–24}

Prior studies have elucidated the existence of a C-terminal binding site on Hsp90 that can be targeted by the development of

inhibitors for the potential treatment of cancer. Although a number of compounds have been prepared, there is currently no binding model to assist in the development of more efficacious inhibitors. Three-dimensional quantitative structure–activity relationship (3D-QSAR) methods were introduced into the analyses and the design of drug molecules in the present study. We have applied two methodologies, comparative molecular field analysis (CoMFA)^{25,26} and comparative molecular similarity indices analysis (CoMSIA),²⁷ to build the 3D-QSAR models based on a set of Hsp90 inhibitors. The established models not only predict the biological activity values of novobiocin derivatives rapidly and accurately but also provide some valuable information in structural modifications for designing new possible lead compound of the inhibitors with higher activity.

2. MATERIAL AND METHODS

2.1. Data Set. The novobiocin derivative inhibitors were derived from the refs 17, 22, and 23, in which some compounds have been removed because there is no determinate activity or have not been tested. Therefore, only 53 compounds were used in this work. The structures of all compounds and their biological activities are listed in Table 1. Inhibitory concentrations (IC₅₀) of these compounds were transformed to negative logarithmic units marked as pIC₅₀. The whole data set was divided into two subsets randomly: the training set of 41 compounds and the test set of 12 compounds (asterisk labeled in Table 1). The training set was

Received: May 20, 2011

Published: July 14, 2011

Table 1. Structures of Novobiocin Derivatives and Predicted Results of pIC₅₀

No.	Exp. ^a	CoMFA		CoMSIA	
		Pred. ^b	Res. ^c	Pred. ^d	Res.

a

b

	n	R ₁	R ₂						
1	a	2	OH	OH	4.97	4.80	0.17	4.99	-0.02
2*	b	2	OH	OH	5.16	4.84	0.32	4.96	0.20
3	a	2	OH	H	5.10	5.14	-0.04	5.02	0.08
4	b	2	OH	H	4.52	4.87	-0.35	4.72	-0.20
5	a	2	H	OH	5.29	5.30	-0.01	5.44	-0.15
6	b	2	H	OH	5.51	5.03	0.48	5.29	0.22
7	b	1	OH	OH	4.84	4.71	0.13	4.70	0.14
8	a	1	H	OH	4.65	4.68	-0.03	4.67	-0.02
9	b	1	H	OH	4.67	4.68	-0.01	4.55	0.12

10

11

12

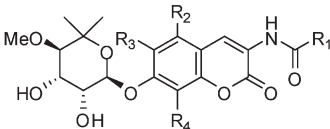
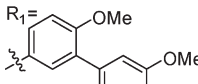
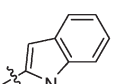
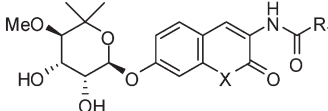
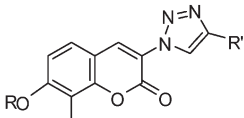
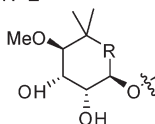
R	R'	R''							
11	A	Ac	Me	6.24	6.21	0.03	6.10	0.14	
12	B	Ac	Me	5.85	5.81	0.04	5.83	0.02	
13*	C	Ac	Me	5.88	6.07	-0.19	5.98	-0.10	
14	D	Ac		6.34	6.29	0.05	6.28	0.06	
15	A	Ac	H	6.25	6.17	0.08	6.22	0.03	
16	B	Ac	H	5.91	5.94	-0.03	5.99	-0.08	
17	C	Ac	H	6.04	5.98	0.06	6.09	-0.05	
18*	A	H	Me	6.12	6.06	0.06	5.89	0.23	
19*	A	H	H	6.33	6.02	0.31	6.02	0.31	
20	B	H	Me	5.33	5.83	-0.50	5.72	-0.39	
21	B	H	H	6.10	5.96	0.14	5.88	0.22	
22	D	H		6.36	6.30	0.06	6.36	0.00	
23	C	H	H	6.12	6.12	0.00	6.04	0.08	

24

25

R ₁	R ₂	R ₃	R ₄						
24	biaryl	H	OMe	Me	4.23	4.10	0.13	4.25	-0.02
25	biaryl	H	O'Pr	Me	4.23	4.12	0.11	4.27	-0.04
26	biaryl	OMe	H	Me	4.25	4.31	-0.06	4.49	-0.24
27	biaryl	H	H	Ph	4.76	4.59	0.17	4.54	0.22
28	biaryl	H	H	OMe	4.86	4.79	0.07	4.75	0.11
29	biaryl	H	H	Et	4.54	4.64	-0.10	4.61	-0.07
30*	2-indole	H	OMe	Me	4.60	4.77	-0.17	4.71	-0.11
31*	2-indole	H	O'Pr	Me	4.68	4.71	-0.03	4.73	-0.05
32	2-indole	OMe	H	Me	5.05	4.92	0.13	4.77	0.28
33	2-indole	H	H	Bn	4.42	4.58	-0.16	4.50	-0.08

Table 1. Continued

No.	Exp. ^a				CoMFA		CoMSIA		
					Pred. ^b	Res. ^c	Pred. ^d	Res.	
<div><div></div><div><div>$R_1=$</div><div>biaryl</div></div><div><div></div><div>2-indole</div></div></div>									
	R ₁	R ₂	R ₃	R ₄					
34	2-indole	H	H	Ph	4.41	4.84	-0.43	4.72	-0.31
35	2-indole	H	H	OMe	5.01	5.00	0.01	4.88	0.13
36*	2-indole	H	H	Et	5.37	4.85	0.52	4.74	0.63
<div></div>									
	R ₁	X							
37	biaryl	N			4.78	4.67	0.11	4.76	0.02
38	biaryl	CH			4.41	4.57	-0.16	4.65	-0.24
<div><div></div><div>$R=E$</div></div>									
	R	R'							
39	OH	phenyl			4.41	4.36	0.05	4.24	0.17
40	OAc	phenyl			4.12	4.28	-0.16	4.19	-0.07
41	OAc	4-methyl-phenyl			4.04	4.13	-0.09	4.09	-0.05
42*	OH	2,4-difluoro-phenyl			4.47	4.34	0.13	4.30	0.17
43	OH	biaryl			4.35	4.38	-0.03	4.42	-0.07
44	OAc	biaryl			4.29	4.33	-0.04	4.26	0.03
45	E	biaryl			4.67	4.74	-0.07	4.59	0.08
46	OH	(E)-2-phenyl-vinyl			4.47	4.35	0.12	4.31	0.16
47*	OAc	(E)-2-phenyl-vinyl			4.19	4.43	-0.24	4.55	-0.36
48*	E	(E)-2-phenyl-vinyl			4.28	4.48	-0.20	4.34	-0.06
49*	OH	2-indole			4.37	4.03	0.34	4.12	0.25
50	OAc	2-indole			4.30	4.17	0.13	4.24	0.06
51*	OH	3-indole			4.88	5.04	-0.16	5.08	-0.20
52	OAc	3-indole			5.19	5.19	0.00	5.20	-0.01
53	OH	3-indole			5.09	5.15	-0.06	5.30	-0.21

^a Experimental pIC₅₀. ^b Predicted by CoMFA. ^c Relative error of (experimental predicted). ^d Predicted by CoMSIA. * The sample of the test set.

employed to construct CoMFA and CoMSIA models, and the test set was used for the validation of established models.

2.2. Molecular Modeling and Alignment. All molecular modeling and calculations were carried out by the Sybyl v6.9 package (Tripos, Inc.), and their energy minimizations were performed using the Tripos force field with the Powell conjugate gradient minimization algorithm, in which a convergence criterion was up to 0.005 kcal/mol Å. Gasteiger–Hückel charge was used to calculate the partial atomic charges. Owing to the highest inhibitory activity in whole data set, compound **22** was used as a template to fit the remaining compounds by using the database align function in Sybyl. The aligned compounds are displayed in Figure 1.

2.3. CoMFA and CoMSIA Descriptors. In order to explore the contributions of various interactions, CoMFA and CoMSIA studies were carried out based on the molecular alignment as described in the Sybyl software.

The CoMFA descriptors, including steric (Lennard-Jones 6-12 potential) and electrostatic (Coulomb potential) field energies between the probe and the test molecule at each lattice intersection, were calculated with a grid step size of 2 Å using sp³ C⁺ as the probe atom with a van der Waals radius of 1.52 Å. The CoMFA fields generated automatically were scaled by the CoMFA-STD method with default energy of 30 kcal/mol.

In CoMSIA models, the descriptors of similarity indices were obtained with the same lattice box used in the CoMFA calculations. Steric, electrostatic, hydrophobic, hydrogen-bond (H-bond) donor, and H-bond acceptor fields were evaluated using the same probe atom in CoMFA analysis. In CoMSIA study, Gaussian-type distance dependence was employed to measure the relative attenuation of the field position of each atom in the lattice and led to much smoother sampling of the fields around the molecules. Generally, CoMSIA similarity indices ($A_{F,k}$) for a

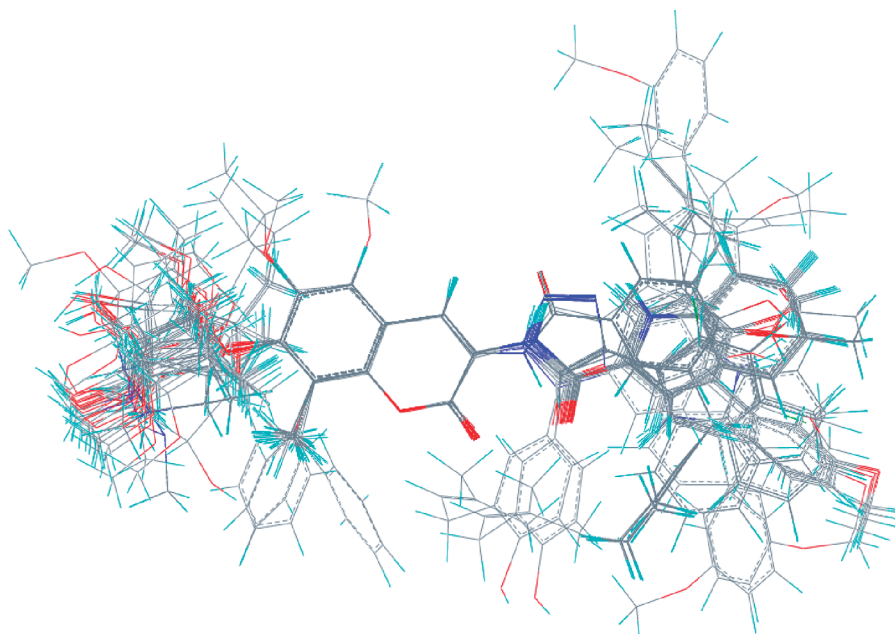


Figure 1. The alignment of all the compounds.

molecule j with atoms i at a grid point q was calculated as follows:

$$A_{F,k}^q(j) = - \sum_i \omega_{\text{probe},k} \omega_{ik} e^{-\alpha r_{iq}^2} \quad (1)$$

where ω_{ik} is the actual value of physicochemical property k of atom i , which is evaluated using the probe atom, and $\omega_{\text{probe},k}$ is the value of the probe atom. At each grid point, a Gaussian-type distance dependence is used between the grid point q and each atom i of the molecule. The default value of 0.3 was used as the attenuation factor α , which showed the steepness of the Gaussian-type function.

2.4. Partial Least-Squares Analysis. Partial least-squares (PLS) regression analyses were implemented with the QSAR module in Sybyl software. To speed up the analysis and reduce the noise, the column filtering was set to 2.0 kcal/mol. The CoMFA and CoMSIA descriptors were denoted as independent variables, and the pIC_{50} values were presented as the respondent variables in PLS regression analysis. The performance of models was indicated with the leave-one-out (LOO) cross-validation.^{26,28} The cross-validated coefficient, q^2 , is regarded as

$$q^2 = 1 - \frac{\sum_{i=1}^n (Y_{\text{predicted}} - Y_{\text{observed}})^2}{\sum_{i=1}^n (Y_{\text{observed}} - Y_{\text{mean}})^2} \quad (2)$$

where $Y_{\text{predicted}}$, Y_{observed} , and Y_{mean} for target property (pIC_{50}) are obtained, respectively. The optimal number of components (ONC) was determined with the highest cross-validated q^2 , and the final PLS regression (noncross-validated conventional analysis) models were established. The statistical parameters for the final PLS models were calculated such as conventional correlation coefficient r^2 , standard error of estimate (SEE), and F -test. The contour maps in the CoMFA and CoMSIA models were generated by the interpolation of the pairwise products between the PLS coefficients and the standard deviations of the corresponding CoMFA or CoMSIA descriptor values.

Table 2. Statistical Parameters for the Final CoMFA and CoMSIA Model

statistical parameters	CoMFA model	CoMSIA model
q^{2a}	0.702	0.707
ONC ^b	5	6
r^{2c}	0.944	0.955
SEE ^d	0.178	0.162
F_{ratio}^e	118.032	119.293
$r^2_{\text{pred}}^f$	0.869	0.855
fraction of field contributions ^g		
steric	0.509	0.152
electrostatic	0.491	0.257
hydrophobic		0.212
donor		0.204
acceptor		0.173

^a Cross-validated correlation. ^b Optimum number of components. ^c Non-cross-validated correlation. ^d Standard error of estimate. ^e F -test value. ^f Predictive r^2 . ^g Field contributions: steric, electrostatic, hydrophobic, H-bond donor, and H-bond acceptor.

3. RESULTS AND DISCUSSION

In order to design higher active possible lead compounds effectively, the CoMFA and CoMSIA models were analyzed, and several important influence factors were obtained. Based on these results, we designed six new novobiocin derivatives with higher predicted activities.

3.1. Reliability of the 3D-QSAR Models. The results obtained from the CoMFA and CoMSIA models are listed in Tables 1 and 2, respectively. The CoMFA model has the cross-validated q^2 of 0.702 with 5 ONC, noncross-validated correlation coefficient r^2 of 0.944, F of 118, and SEE of 0.178. The CoMSIA model has the cross-validated q^2 of 0.707 with 6 components, noncross-validated r^2 of 0.955, F of 119, and SEE of 0.162. These statistic parameters indicate that the CoMFA and CoMSIA models are reliable. To validate the predictive capability of these models, the

12 compounds not used in the construction of CoMFA and CoMSIA models were collected as the test set. The predicted results for the test set are also listed in Table 1 (asterisk labeled). The r^2_{pred} for the test set with CoMFA and CoMSIA models is 0.869 and 0.885, respectively. Testing results also indicate that both CoMFA model and CoMSIA model have satisfactory predictive capability. The correlation between the predicted activities and the experimental activities is depicted in Figure 2. It can be seen from Figure 2 that the predicted pIC_{50} values agree well with the experimental values in a tolerable error range.

In CoMFA model, the steric field descriptors explain 50.9% of the variance, while the electrostatic descriptors explained 49.1%. In CoMSIA model, corresponding to the steric, electrostatic, hydrophobic, H-bond donor, and H-bond acceptor fields, the contributions of variables are 15.4, 25.7, 21.2, 20.4, and 17.3%, respectively. Although both CoMFA and CoMSIA models had satisfactory predictive capability, the CoMSIA model can explain more structural information, owing to the importance effects of the hydrophobic and H-bonds for the activities of these

inhibitors. In the CoMFA model, the contribution of steric field is slightly larger than that of electrostatic field; however, the situation is the opposite in the CoMSIA model. This can be explained by the introducing of hydrophobic field and also by the fact that the steric field is correlated with hydrophobic field to some extent.

3.2. Graphical Interpretation of CoMFA and CoMSIA Model. **3.2.1. Graphical Interpretation of CoMFA Model.** In CoMFA and CoMSIA models, contour maps can provide useful information to understand the key structural features responsible for the activity. The contour maps of the models can clearly show how the different substituents of potent inhibitors influence the inhibitory activity.

The CoMFA contour maps of steric and electrostatic field are shown in Figure 3, in which compound **22** is displayed with aid of visualization. In the CoMFA steric field, the green contours (contribution level of 80%) represent a steric group that confers an increased activity, while yellow contours (contribution level of 20%) represent a bulky group that results in a decreased

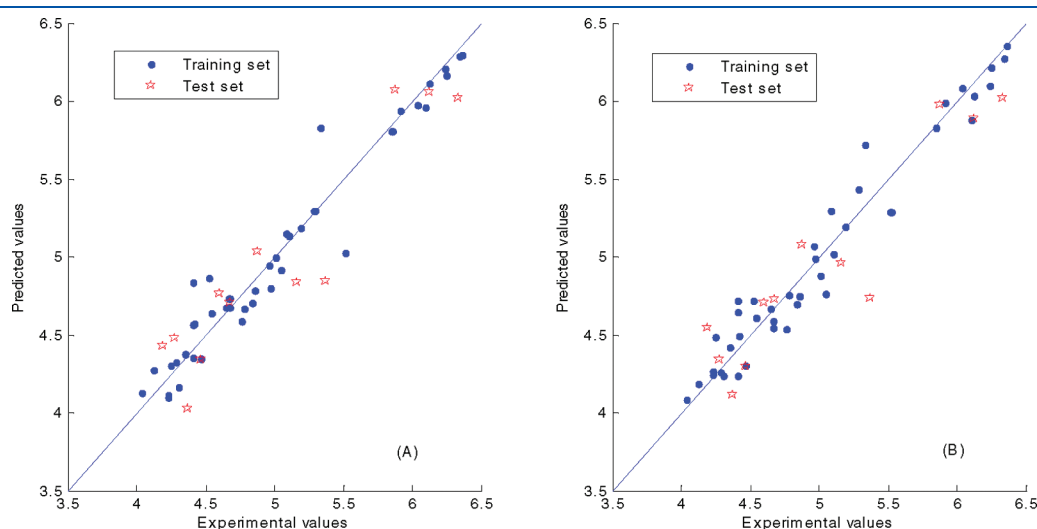


Figure 2. The plot of the predicted pIC_{50} versus the experimental pIC_{50} for the CoMFA (A) and CoMSIA (B) models.

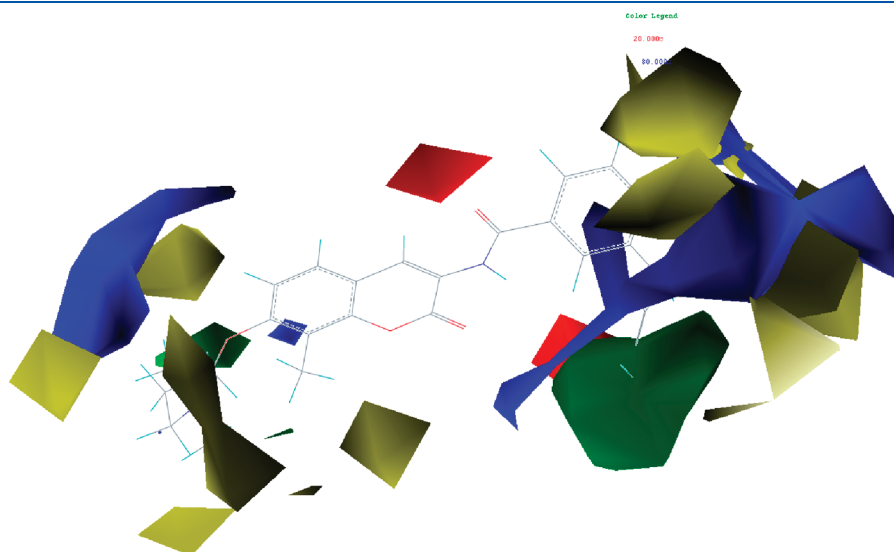


Figure 3. CoMFA StDev * coeff contour plots.

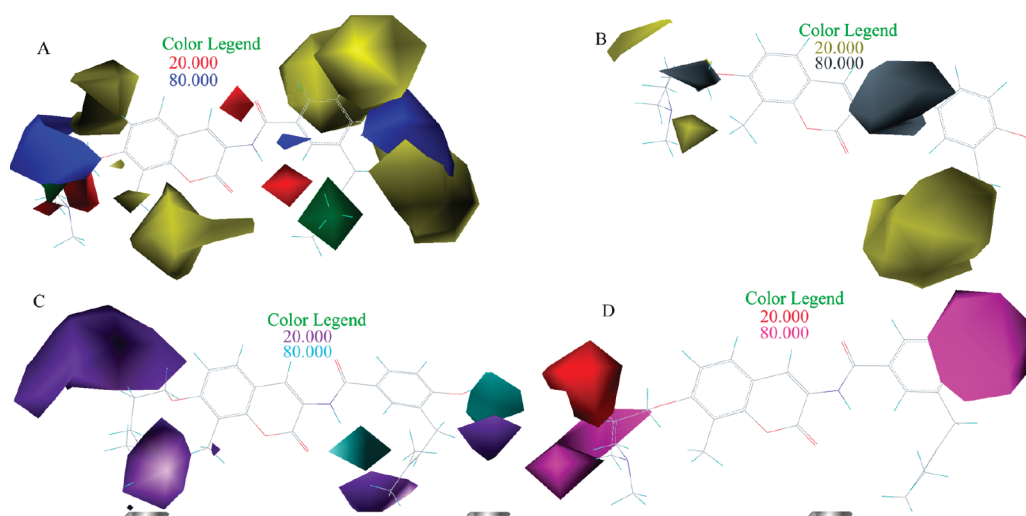


Figure 4. CoMSIA StDev * coeff contour plots. Contour maps for (A) steric field and electrostatic field; (B) hydrophobic field; (C) H-bond donor field; and (D) H-bond acceptor field.

activity. Similarly, the blue contours indicate the regions where the addition of electropositive substituents increases activity (contribution level of 80%), and red contours indicate the regions where the addition of electronegative substituents increases activity (contribution level of 20%). As Figure 3 shows, the contour map of the steric field in CoMFA model, a large region of green contour near the three-substituent of benzamide, indicating that a steric bulk is favored there. This can be explained by the fact that molecules with the replacement of three positions with $-\text{CH}_2\text{CH}=\text{C}(\text{CH}_3)_2$ group of benzamide all have high activities. A moderate green contour near the $-\text{R}$ substituent suggests that a bulky group would increase the activity. A large region of yellow contour near the 4,5-substituents of benzamide suggests that bulky group would decrease the activity. This can be explained by the fact that replacement of $-\text{CH}_3$ with $-\text{H}$ group enhances the activity (compounds: **23** > **17**; **22** > **14**; and **21** > **16**).

In the contour map of the electrostatic field in CoMFA model (shown in Figure 3), a red area near the oxygen of the benzamide and a moderate region of blue contour near the benzene ring indicate that benzamide is critical for activity, which is consistent with the results of Yu and co-workers' study.²⁴ Amide is an electron-withdrawing group, which reduces the electron density in the benzene ring.

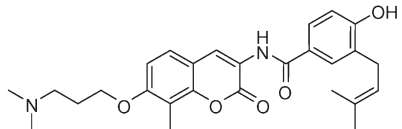
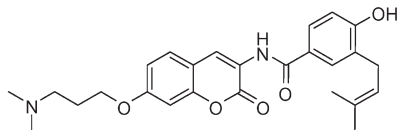
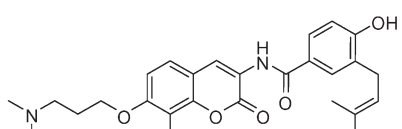
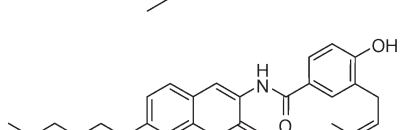
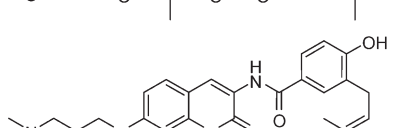
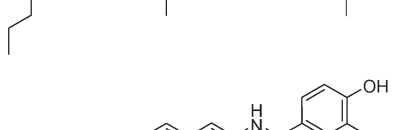
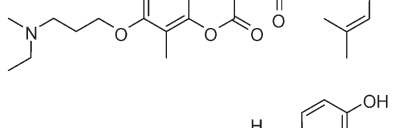
3.2.2. Graphical interpretation of CoMSIA model. The steric and electrostatic field distributions of CoMSIA, depicted in Figure 4A, are generally in accordance with the field distributions of CoMFA map (Figure 3). In the contour map of the steric field, the large regions of yellow contour near the R_3 and R_4 in benzene ring suggest that bulky groups would decrease the activity. These are in agreement with the fact that the activity of compound **27** ($\text{R}_4\text{--OMe}$) is lower than that of compound **28** ($\text{R}_4\text{--Ph}$), and the activity of compound **34** ($\text{R}_4\text{--Ph}$) is lower than that of compound **36** ($\text{R}_4\text{--Et}$). The slight differences in steric field are attributed to the introduction of hydrophobic field. The hydrophobic contour map of CoMSIA model is displayed in Figure 4B. Yellow (the contribution level of 80%) and gray (the contribution level of 20%) contours indicate the regions where hydrophobic and hydrophilic groups are preferred, respectively. A large region of the yellow contour near the

3-substituent of benzamide indicates that a hydrophobic group is favored there, which is consistent with the conclusion of steric field. It has been proposed that novobiocin may antagonize the Hsp90 function by inducing a conformational change that results in separation of the homodimeric C-terminal domains and subsequent release of substrate.²⁹ And it is in agreement with the result obtained by M. Sgobba et al. that the benzamide in novobiocin derivatives makes hydrophobic contact with Ala629 and Tyr627 of Hsp90.¹⁵ The gray contour map located around the amide suggests that hydrophobic groups would decrease the activity. As a consequence, amide is a strong hydrophilic group, and therefore it is possible that amide is easy to make H-bonds with amino acid residues and water molecules in Hsp90.

The CoMSIA contour map of the H-bond donor and H-bond acceptor fields is shown in Figure 4C and D, respectively. Cyan contours (contribution level of 80%) indicate that H-bond donor groups increase activity, and purple contours (contribution level of 20%) suggest that H-bond donor groups decrease activity. The cyan contours near the nitrogen atom and 4-OH of benzamide suggest that H-bond donor groups are favored there. These can be explained that both amide and 4-OH may make H-bonds with amino acids residues and water molecules of Hsp90 as H-bond donors. And the result is also in accordance with the result obtained by M. Sgobba et al. that the hydroxyl group of the benzamide H-bonds with Lys582 and Glu679 of Hsp90.¹⁵ The purple contours near the noviose and 3-substituents of benzamide suggest that H-bond donor groups are disfavored there. Magenta contours (contribution level of 80%) indicate the region where H-bond acceptor groups increase activity, and red contours (contribution level of 20%) represent the region where H-bond acceptor groups decrease activity. The large regions of magenta contour around 4-OH of benzamide and hydroxyls of noviose suggest that H-bond acceptor groups are favored there. The region of red contour around $-\text{CH}_3$ of noviose suggests that an H-bond acceptor group is disfavored there. The results obtained from contour maps of the H-bond donor and H-bond acceptor field are consistent. Interestingly, 4-OH of benzamide may form H-bonds not only as a hydrogen acceptor but also as a hydrogen donor. And the results are in

agreement with structure–activity relationship (SAR) hypotheses, which show that a group with H-bond donor and acceptor

Table 3. Structures of Compound 22 and Designed Novobiocin Derivatives and Predicted Results of pIC_{50}

No.		Exp. ^a	Pred. ^b	Pred. ^c
22		6.36	6.30	6.36
54			6.20	6.32
55			6.30	6.37
56			6.21	6.33
57			6.25	6.30
58			6.54	6.35
59			6.11	6.21

^a Experimental pIC_{50} . ^b Predicted by CoMFA. ^c Predicted by CoMSIA.

capabilities on the aryl substituent increases inhibitory activity of C-terminal inhibitors.³⁰

3.3. Summary of SAR. Based on the above discussion, the steric, electrostatic, hydrophobic, H-bond donor, and H-bond acceptor fields are all important for the activity. The benzamide is very important for cytotoxic activity. The amine is H-bond donor, and 4-OH is not only a hydrogen acceptor but also a hydrogen donor. Steric bulk of 3-substituents of benzamide is favored there, but bulky groups of 4, 5- substituents of benzamide would decrease the activity, which is not favored there. Although the oxygen atoms of coumarin are H-bond acceptors, they are difficult to form H-bonds, which may be due to a steric effect; R_4-CH_3 of coumarin ring increases inhibition. The hydroxyls of noviose are H-bond acceptors, and bulky groups of noviose substituents would decrease the activity. However, bulky group of $-R$ substituent would increase the activity.

3.4. Design of New Derivatives. Based on the foregoing analyses, the CoMFA and CoMSIA contour maps offer some valuable information for us to design new similar novobiocin derivatives with higher activity. Here, we designed six new molecules, and predicted their activities using the CoMFA and CoMSIA models. The designed molecules were checked with docking study, the obtained results are very similar to that of compound 22. The structures of the six compounds and their predicted activities are listed in Table 3. From Table 3, the inhibitory activity of molecule 58 with the larger $-R$ substituent is higher than that of molecule 22. But when $-R$ substituent is too bulky, the derivative has lower activity (compounds: 59 < 22). As mentioned earlier, R_4-CH_3 of coumarin ring increases inhibition, $R_4-CH_2CH_3$ also can increase the activity (compounds: 55 > 22 > 54).

The several molecular properties of six compounds calculated using the HyperChem package (the simple molecular modeling and simulation software that lets you perform complex chemical calculations, Hypercube, Inc.) are listed in Table 4. From the table, we can see that the free energy, binding energy, and heat of formation of the new molecule are as much as molecule 22, even smaller. And the physicochemical properties, such as the surface area (Grid), volume, and Log P of the new molecules, are similar to that of molecule 22. All the above indicate that these designed molecules can be synthesized possibly and can have a steady existence.

The six new molecules have higher predicted activity, and their behaviors coincide with the results of CoMFA and CoMSIA models, which provide the potential anticancer drug leads for further research.

Table 4. Molecular Properties of Compound 22 and Designed Novobiocin Derivatives^a

no.	surface area (grid) [\AA^2]	volume [\AA^3]	log P	free energy [kcal/mol]	binding energy [kcal/mol]	heat of formation [kcal/mol]
22	826.00	1397.46	3.48	−126486.42	−6950.09	−145.01
54	805.38	1356.55	3.01	−123038.34	−6670.05	−140.05
55	823.03	1431.10	3.87	−129933.69	−7229.34	−149.16
56	803.20	1345.20	3.33	−125713.29	−6608.69	−184.24
57	883.20	1507.60	4.29	−133386.17	−7513.78	−158.51
58	852.46	1451.75	3.82	−129937.48	−7233.13	−152.94
59	874.83	1494.08	4.23	−133386.46	−7514.08	−158.80

^a Note: Surface area (grid), the more accurate surface area of molecule calculated with grid method. Volume, the volume of molecule calculated with grid method. Log P, the log of the octanol–water partition coefficient. Free energy, Helmholtz free energy (A) calculated by energy (E) and entropy (S) with $A = E - TS$. Binding energy, the energy of the attraction between an electron in an atomic orbital and the nucleus of the same atom. Heat of formation, calculated with semi-empirical method.

4. CONCLUSIONS

By means of 3D-QSAR studies on a series of Hsp90 inhibitors, the CoMFA and CoMSIA models established are quite reliable, and their capabilities of prediction are satisfactory. The 3D-QSAR models also reveal several important points. Benzamide is more important for cytotoxic activity, and bulky groups of coumarin ring are not favored. R₄—CH₃ of coumarin ring increases Hsp90 inhibition. The hydroxyls of noviose are H-bond acceptors, and bulky groups of noviose substituents would decrease the activity. Based on the analysis of 3D-QSAR models, six new possible lead compounds with higher activity were designed. Our study indicates that 3D-QSAR models can provide efficient suggestions for the further modification of drug molecules.

AUTHOR INFORMATION

Corresponding Author

*E-mail: zhaihl@163.com. Telephone: +86 931 8912596.

REFERENCES

- (1) Paul Workman, P. Pharmacogenomics in cancer drug discovery and development inhibitors of the Hsp90 molecular chaperone. *Cancer Detect. Prev.* **2002**, 26, 405–410.
- (2) Burlison, J.; Avila, C.; Vielhauer, G.; Lubbers, D.; Holzbeierlein, J.; Blagg, B. Development of novobiocin analogues that manifest antiproliferative activity against several cancer cell lines. *J. Org. Chem.* **2008**, 73, 2130–2137.
- (3) Scheibel, T.; Buchner, J. The Hsp90 complex—a super-chaperone machine as a novel drug target. *Biochem. Pharmacol.* **1998**, 56, 675–682.
- (4) Neckers, L.; Schulte, T.; Mimnaugh, E. Geldanamycin as a potential anti-cancer agent: its molecular target and biochemical activity. *Invest. New Drugs* **1999**, 17, 361–373.
- (5) Maloney, A.; Workman, P. HSP90 as a new therapeutic target for cancer therapy: the story unfolds. *Expert Opin. Biol. Ther.* **2002**, 2, 3–24.
- (6) Isaacs, J. S.; Xu, W.; Neckers, L. Heat shock protein 90 as a molecular target for cancer therapeutics. *Cancer Cell* **2003**, 3, 213–217.
- (7) Roe, S.; Prodromou, C.; O'Brien, R.; Ladbury, J.; Piper, P.; Pearl, L. Structural basis for inhibition of the Hsp90 molecular chaperone by the antitumor antibiotics radicicol and geldanamycin. *J. Med. Chem.* **1999**, 42, 260–266.
- (8) Whitesell, L.; Lindquist, S. HSP90 and the chaperoning of cancer. *Nat. Rev. Cancer* **2005**, 5, 761–772.
- (9) Avila, C.; Hadden, M.; Ma, Z.; Kornilayev, B.; Ye, Q.; Blagg, B. High-throughput screening for Hsp90 ATPase inhibitors. *Bioorg. Med. Chem. Lett.* **2006**, 16, 3005–3008.
- (10) Whitesell, L.; Bagatell, R.; Falsey, R. The stress response: implications for the clinical development of hsp90 inhibitors. *Curr. Cancer Drug Targets* **2003**, 3, 349–358.
- (11) Powers, M.; Workman, P. Inhibitors of the heat shock response: biology and pharmacology. *FEBS Lett.* **2007**, 581, 3758–3769.
- (12) Le Bras, G.; Radanyi, C.; Peyrat, J.; Brion, J.; Alami, M.; Marsaud, V.; Stella, B.; Renoir, J. New novobiocin analogues as antiproliferative agents in breast cancer cells and potential inhibitors of heat shock protein 90. *J. Med. Chem.* **2007**, 50, 6189–6200.
- (13) Marcu, M.; Schulte, T.; Neckers, L. Novobiocin and related coumarins and depletion of heat shock protein 90-dependent signaling proteins. *JNCL, J. Natl. Cancer Inst.* **2000**, 92, 242–248.
- (14) Marcu, M.; Chadli, A.; Bouhouche, I.; Catelli, M.; Neckers, L. The heat shock protein 90 antagonist novobiocin interacts with a previously unrecognized ATP-binding domain in the carboxyl terminus of the chaperone. *J. Biol. Chem.* **2000**, 275, 37181–37186.
- (15) Sgobba, M.; Forestiero, R.; Degliesposti, G.; Rastelli, G. Exploring the Binding Site of C-Terminal Hsp90 Inhibitors. *J. Chem. Inf. Model.* **2010**, 50, 1522–1528.
- (16) Burlison, J.; Neckers, L.; Smith, A.; Maxwell, A.; Blagg, B. Novobiocin: redesigning a DNA gyrase inhibitor for selective inhibition of hsp90. *J. Am. Chem. Soc.* **2006**, 128, 15529–15536.
- (17) Donnelly, A.; Mays, J.; Burlison, J.; Nelson, J.; Vielhauer, G.; Holzbeierlein, J.; Blagg, B. The design, synthesis, and evaluation of coumarin ring derivatives of the novobiocin scaffold that exhibit antiproliferative activity. *J. Org. Chem.* **2008**, 73, 8901–8920.
- (18) Radanyi, C.; Le Bras, G.; Marsaud, V.; Peyrat, J.; Messaoudi, S.; Catelli, M.; Brion, J.; Alami, M.; Renoir, J. Antiproliferative and apoptotic activities of tosylcyclonovobiocic acids as potent heat shock protein 90 inhibitors in human cancer cells. *Cancer Lett.* **2009**, 274, 88–94.
- (19) Hengeller, C.; Licciardello, G.; Tudino, V.; Marcelli, E.; Virgilio, A. Isolation and Characterization of an Actinophage (Phage A) active against a Strain of Streptomyces producing Novobiocin. *Nature* **1965**, 205, 418–419.
- (20) Schwartz, G.; Teicher, B.; Eder, J.; Korbut, T.; Holden, S.; Ara, G.; Herman, T. Modulation of antitumor alkylating agents by novobiocin, topotecan, and lonidamine. *Cancer Chemother. Pharmacol.* **1993**, 32, 455–462.
- (21) Nordenberg, J.; Albukrek, D.; Hadar, T.; Fux, A.; Wasserman, L.; Novogrodsky, A.; Sidi, Y. Novobiocin-induced anti-proliferative and differentiating effects in melanoma B16. *Br. J. Cancer* **1992**, 65, 183–188.
- (22) Zhao, H.; Kusuma, B. R.; Blagg, B. S. J. Synthesis and Evaluation of Noviose Replacements on Novobiocin That Manifest Antiproliferative Activity. *ACS Med. Chem. Lett.* **2010**, 1, 311–315.
- (23) Peterson, L.; Blagg, B. Click Chemistry to Probe Hsp90: Synthesis and Evaluation of a Series of Triazole Containing Novobiocin Analogues. *Bioorg. Med. Chem. Lett.* **2010**, 20, 3957–3960.
- (24) Yu, X.; Shen, G.; Neckers, L.; Blake, H.; Holzbeierlein, J.; Cronk, B.; Blagg, B. Hsp90 inhibitors identified from a library of novobiocin analogues. *J. Am. Chem. Soc.* **2005**, 127, 12778–12779.
- (25) Cramer, Richard D., I.; Patterson, D. E.; Bunce, J. D. Comparative Molecular Field Analysis (CoMFA). 1. Effect of Shape on Binding of Steroids to Carrier Proteins. *J. Am. Chem. Soc.* **1988**, 110, 5959–5967.
- (26) Cramer, R., III; Bunce, J.; Patterson, D.; Frank, I. Crossvalidation, bootstrapping, and partial least squares compared with multiple regression in conventional QSAR studies. *Quant. Struct.-Act. Relat.* **1988**, 7, 18–25.
- (27) Klebe, G.; Abraham, U.; Mietzner, T. Molecular similarity indices in a comparative analysis (CoMSIA) of drug molecules to correlate and predict their biological activity. *J. Med. Chem.* **1994**, 37, 4130–4146.
- (28) Wold, S. Cross-validatory estimation of the number of components in factor and principal components models. *Technometrics* **1978**, 20, 397–405.
- (29) Allan, R. K.; Mok, D.; Ward, B. K.; Ratajczak, T. Modulation of Chaperone Function and Cochaperone Interaction by Novobiocin in the C-terminal Domain of Hsp90. *J. Biol. Chem.* **2006**, 281, 7161–7171.
- (30) Donnelly, A.; Blagg, B. S. J. Novobiocin and additional inhibitors of the Hsp90 C-terminal nucleotide-binding pocket. *Curr. Med. Chem.* **2008**, 15, 2702–2717.